V International Conference on Computational Methods for Coupled Problems in Science and Engineering
COUPLED PROBLEMS 2013
S. Idelsohn, M. Papadrakakis and B. Schrefler (Eds)

COUPLED THERMO-HYDRO-MECHANICAL MODELLING OF CRACK DEVELOPMENT ALONG FOSSIL DINOSAUR'S FOOTPRINTS IN SOFT COHESIVE SEDIMENTS

LONG NGUYEN-TUAN*, HANNA VIEFHAUS*, MARIA DATCHEVA† AND TOM SCHANZ*

*Chair for Foundation Engineering, Soil and Rock Mechanics
Ruhr-Universität-Bochum, Germany
Universitätsstr. 150, IA 4, 44780 Bochum
e-mail: [long.nguyentuan; hanna.viefhaus; tom.schanz]@rub.de, web page: http://www.gbf.rub.de/

†Institute of Mechanics - Bulgarian Academy of Sciences
Acad. G. Bontchev, block 4, 1113 Sofia Bulgaria
e-mail: datcheva@imbm.bas.bg - web page: http://www.imbm.bas.bg/112

Key words: coupled Thermo-Hydro-Mechanical (THM) modelling, dinosaur's footprints, 3D finite element analysis, crack analysis.

Abstract. The fossil footprints have been used to back calculate the properties of the soil in the Age of Dinosaurs. The interpretation of fossil footprints requires the simulation of the processes during as well as after the footprint was generated. Some radial and circumferential cracks were observed occurring on track walls of the footprints. It is supposed that the origin of these cracks can be elucidated by means of footprint's drying after the footprint is generated.

In order to verify this hypothesis and to allow for a precise interpretation of the dinosaur tracks, a series of laboratory and numerical simulation tests was carried out. The tests were designed to mimic the shape evolution of the footprint of the dinosaur during drying. Within the experiments the change of environmental humidity and temperature was monitored and recorded. The laboratory experiment showed that both the radial and circumferential cracks appear during the drying process.

The numerical simulation has been performed to better understand and to account for the cracking mechanism in dinosaur's tracks. In this study the behaviour of a silty soil during drying is numerically simulated by means of a 3D model and performing coupled thermo-hydro-mechanical analysis utilizing the finite element program CODE_BRIGHT. Based on the analysis of the tensile stresses along the sample, it was found that the highest tensile stress is on the track wall and it is due to soil shrinkage. It can be concluded that the high tensile stress induced during drying is the most possible reason for cracks to appear in radial and circumferential direction along the foot's imprint.

1 INTRODUCTION

The study of fossil footprints plays an important role for investigation of the animal characteristics, behaviour and its natural environment during the Dinosaur Age. Many paleontologists contributed studies on the morphology of the fossil footprints, the motion of the vertebrates and the sediment structure based on analysis of the imprinting process [7, 8, 9].

This paper contributes to the analysis of the change of the mechanical properties of soil composing the footprint starting from the initial saturated sediment and posterior imprinting process. If the sediment is soft enough to allow the foot sinking to a certain depth, there will be formed a vertical wall due to the pail up from the true footprint to the soil surface. This vertical wall is termed a track wall [9]. Palaeontologists have discovered many track walls on which fractures were observed at radial direction and along the contour around the imprint. Figure 1 presents the footprints of dinosaurs from Colorado, USA, showing the existence of many fractures on the track wall of the footprints. A question now arises what physical conditions and mechanisms caused these fractures. It is to be mentioned that a crack may be formed at different periods – during the imprinting period (peak weight-bearing [7]) or during the period of track drying, and because of the tectonic movement and weathering. Cracks during the peak weight-bearing period were observed in several virtual experiments [7, 8], where fractures have circumferential shape surrounding the footprint. This fact was explained by the shearing in the thrust shear zone induced by the dynamic movement of the dinosaur's foot. Another hypothesis is that the tectonic movement induced shear and tension forces in the rock mass that initiated the fractures. Theories explaining the fracture process were analysed using stress approach and energy approach [2] and modelled accounting for the pre-existing flaw [6]. However, the tectonic cracks have different aspects compared to the cracks found at the track wall of the dinosaur footprints. It is supposed that the origin of track wall fractures/cracks can be understood by means of soil drying after the footprint is generated. Therefore, in this study an experiment was designed to simulate the footprint alteration with the progress of the drying process.

The paper is focused on the application of a thermo-hydro-mechanical model to qualitatively interpret the cracking initiation phenomenon. The analysis of the tension stress at the soil surface made it possible to explain the crack initialisation. Therefore a 3-dimensional analysis based on THM numerical simulation was performed. The footprint behaviour during drying has been numerically simulated in 3D by means of coupled THM analysis available in CODE_BRIGHT program [3]. The stress-strain behaviour is reproduced by a thermo-elasto-plastic model being a modification of the Barcelona Basic Model [1] accounting soil swelling and shrinking with the change of water content and temperature [5].

(a) (b)

Figure 1: Dinosaur footprints: (a) Dinosaur's tracks from Copper Ridge in Arches-Nationalpark, Colorado USA, source: wordpress.com (b) A small Dino-track from Garmin Colorado, source: Earthcache.

2 EXPERIMENTAL MOTIVATION

A soil ring sample having approximately the same dimensions as the dinosaur's footprint was prepared to mimic qualitatively the formation and the alteration of the footprint after the weight-bearing period. A heaved ring aimed to simulate the track wall was formed reproducing the track wall geometry. The material of the soil ring was a silty clay that was initially water saturated. The soil ring and the base are shown in Fig. 2(a). The inner diameter is 40 cm, the outer diameter is 80 cm. The height of the ring is 6 cm, the thickness of the square base is 12 cm. The environmental humidity and temperature were varied during the experiment and two stages of the experiment can be distinguished. In the first stage, the specimen was situated for 20 days in laboratory conditions at temperature 20°C and relative humidity of 53%. In the second stage, the specimen was exposed to the sun for 20 days. Under the change of environment the soil specimen was drying by soil-water evaporation.

The laboratory experiment showed that during the drying process both the radial and circumferential cracks appeared. The cracks that were formed after 40 days are presented in Fig. 2(b). It can be seen that radial cracks appeared on the ring, and the circumferential cracks appeared at the outside and inside edges of the ring. In the drying process the soil water was released by evaporation. The reduction of soil pore water induced shrinkage of the specimen. The magnitude of this shrinkage is different along the specimen, e.g. the shrinkage at the surface of the specimen and inside the specimen is not the same. This difference induces tension stress on the surface of the specimen. If the tension stress is higher than the tensile strength of the soil, cracks will occur.

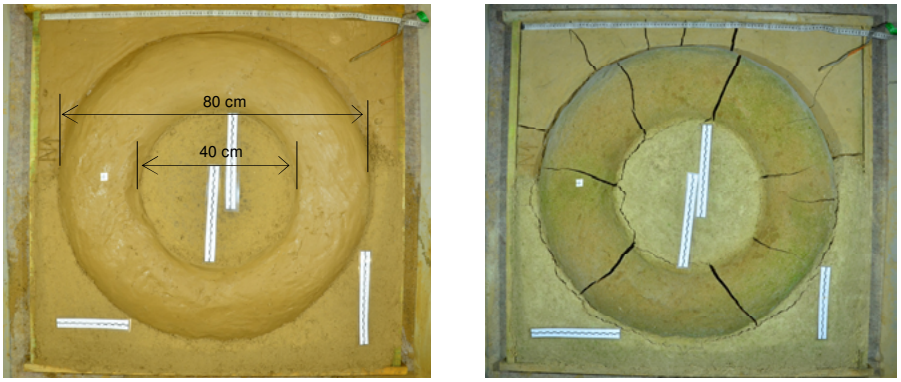

(a) (b)

Figure 2: Experiment to mimic the behaviour of the dinosaur's footprint: (a) initial state, (b) state after 40 days.

3 COUPLED THERMO-HYDRO-MECHANICAL ANALYSIS

A thermo-hydro-mechanical analysis of expansive soil, which is available in the finite element code in CODE_BRIGHT [3], was used for numerical simulation of the performed experiment. The equations that govern the THM response can be categorised into four main groups, namely, balance equations, constitutive equations, equilibrium restrictions and definition constraints. The balance equations can be seen in [12, 11]. The constitutive relations used for the THM numerical simulation are presented in the following part.

3.1 Constitutive equations of the coupled thermo-elasto-plastic model

For mechanical stress-strain behaviour thermo-elasto-plastic (TEP) model is adopted. It is presented in an incremental form and the increment of the strain as a sum of the increments of the elastic, $d\varepsilon^e$, and plastic, $d\varepsilon^p$, strains:

$$d\boldsymbol{\varepsilon} = d\boldsymbol{\varepsilon}^e + d\boldsymbol{\varepsilon}^p \tag{1}$$

Following the two stress variable concept in unsaturated soil mechanics, the elastic part of the strain increment is taken to be the sum of the increments of suction induced $\boldsymbol{\varepsilon}^{s-e}$, net stress induced $\boldsymbol{\varepsilon}^{\sigma-e}$ and the strain increment due to temperature change $d\boldsymbol{\varepsilon}^{T-e}$. The final relation for the elastic strain increment reads:

$$d\boldsymbol{\varepsilon}^e = d\boldsymbol{\varepsilon}^{\sigma-e} + d\boldsymbol{\varepsilon}^{s-e} + d\boldsymbol{\varepsilon}^{T-e} \tag{2}$$

The nonlinear elastic law for the volumetric strain induced by the net stress is expressed in Eq. 3.

$$d\varepsilon_v^{\sigma-e} = \frac{\kappa_i(s)}{1+e}\,\frac{dp'}{p'} \quad \text{and} \quad p' = p - \max(P_g, P_l) \tag{3}$$

$$\kappa_i(s) = \begin{cases} \kappa_{io}\,(1+\alpha_i\,s) & \text{if } 1+\alpha_i\,s \geq 0.001 \\ 0.001\,k_{io} & \text{if } 1+\alpha_i\,s < 0.001 \end{cases} \tag{4}$$

where p is the mean total stress, p' is the mean net stress in unsaturated state or effective stress in saturated state, P_g and P_l are gas pressure and liquid pressure, e is the void ratio, κ_{io} and α_i are model parameters.

Suction and temperature induce only volumetric strains with constitutive equations given as follows:

$$d\varepsilon_v^{s-e} = \frac{\kappa_s(p',s)}{1+e}\frac{ds}{s+p_{at}} \quad ; \quad d\varepsilon_v^{T-e} = \alpha_o\,dT \tag{5}$$

with

$$\kappa_s(p',s) = \kappa_{so}\kappa_{sp}\ \exp\,(\alpha_{ss}\,s) \tag{6}$$

and

$$\kappa_{sp} = \begin{cases} 1+\alpha_{sp}\ln\left(\dfrac{10^{-20}}{p_{ref}}\right) & \text{if } p' \leq 10^{-20} \\ 0 & \text{if } p' \geq p_{ref}\exp\left(\dfrac{-1}{\alpha_{sp}}\right) \\ 1+\alpha_{sp}\ln\left(\dfrac{p'}{p_{ref}}\right) & \text{elsewhere} \end{cases} \tag{7}$$

The parameters involved are: α_o is for the elastic thermal strain; κ_{so} is the elastic stiffness parameter in changing of suction at zero net stress; p_{at} is the atmospheric pressure; α_{ss} and α_{sp} are model parameters. The elastic slope κ_i and κ_s may be considered not dependent on temperature in case of moderate temperature gradients.

The yield surface in TEP model is given in the deviatoric plane $p-q$ via the following equation:

$$F = q^2 - M^2\,(p'+p_s)\,(p_o-p') = 0 \tag{8}$$

where $q = \sqrt{\dfrac{3}{2}\,\boldsymbol{\sigma}^D : \boldsymbol{\sigma}^D}$, with deviatoric stress defined as $\boldsymbol{\sigma}^D = \boldsymbol{\sigma}' - \dfrac{1}{3}\boldsymbol{\sigma}' : \boldsymbol{I}$. The pre-consolidation pressure p_o depends on suction and according to [1] it is defined as:

$$p_o = p^c\left(\frac{p_o^*}{p^c}\right)^{\dfrac{\lambda\,(0)-\kappa_{io}}{\lambda\,(s)-\kappa_{io}}} \tag{9}$$

where p^c is a reference pressure, p_o^* is the pre-consolidation pressure at the saturated state, $\lambda(0)$ is the plastic stiffness parameters for the change in effective stress at saturated state.

The stiffness parameter for the change in the mean net stress at given suction is defined by:

$$\lambda(s) = \lambda(0)\left[(1-r)\exp(-\beta s) + r\right] \tag{10}$$

where r and β are model parameters.

The tensile strength p_s is proportional to suction and is a given function of temperature:

$$p_s = p_{s0} + k\, s \exp(-\rho \Delta T) \quad \text{and} \quad \Delta T = T - T_{ref} \tag{11}$$

where k is the parameter that takes into account the increase of tensile strength due to suction, p_{s0} is tensile strength in saturated state, ρ is a parameter that takes into account the decrease of the tensile strength due to temperature increase, T_{ref} is reference temperature.

The isotropic hardening depends on the plastic volumetric strain according to:

$$dp_o^* = \frac{1+e}{\lambda(0) - \kappa_{io}}\, p_o^*\, d\varepsilon_v^p \tag{12}$$

3.2 Constitutive equations of the hydraulic model

Mass or liquid transfer is realised via advective flow and diffusion. Both components are considered in this analysis.

The advective flow of the water phase is described by the generalized Darcy's law:

$$\boldsymbol{q}_l = -\frac{\boldsymbol{k} k_{rl}}{\mu_l}\left(\nabla P_l - \rho_l \boldsymbol{g}\right) \tag{13}$$

where μ_l is the dynamic viscosity of the pore liquid, $\boldsymbol{g}$ is the gravity acceleration, ρ_l is the liquid density. The tensor of intrinsic permeability $\boldsymbol{k}$ is supposed to depend on porosity according to the Kozeny's model:

$$\boldsymbol{k} = \boldsymbol{k}_o \frac{\phi^3}{(1-\phi)^2} \frac{(1-\phi_o)^2}{\phi_o^3} \tag{14}$$

where ϕ is the porosity, ϕ_o is a reference porosity, $\boldsymbol{k}_o$ is the intrinsic permeability for matrix with porosity ϕ_o. The relative permeability k_{rl}, is derived using the Mualem-van Genuchten closed form model, [15]:

$$k_{rl} = \sqrt{S_e}\left(1 - \left(1 - S_e^{1/\lambda}\right)^{\lambda}\right)^2 \tag{15}$$

where λ is a shape parameter for the retention curve and S_e is defined as:

$$S_e = \frac{S_l - S_{rl}}{S_{ls} - S_{rl}} = \left(1 + \left(\frac{P_g - P_l}{P}\right)^{\frac{1}{1-\lambda}}\right)^{-\lambda} \quad \text{and} \quad P = P_0\left(\frac{\sigma_T}{\sigma_{T0}}\right) \tag{16}$$

where S_l, S_{ls} and S_{rl} are the current, the maximum and the residual liquid degree of saturation, P_0 is a model parameter, σ_T is surface tension of liquid and $\sigma_T 0$ is surface tension of liquid at which P_0 was measured. According to [13] σ_T is calculated by the empirical relation:

$$\sigma_T = 0.03059 \exp\left(\frac{252.93}{273.15 + T}\right) \tag{17}$$

The molecular diffusion of the vapour in air is governed by the Fick's law. Fick's law is adopted to define The equation for the diffusive flux of the water vapour $\boldsymbol{i}^v$ reads:

$$\boldsymbol{i}^v = -\left(\phi \rho_v S_l D_m \boldsymbol{I}\right) \nabla \omega^v \tag{18}$$

where ρ_v is the vapour density, ω^v is the mass fraction of the vapour, $\boldsymbol{I}$ is the identity matrix and D_m is the diffusion coefficient of vapour in m^2/s and is defined by:

$$D_m = \tau D \frac{(273.15 + T)^n}{P_g} \tag{19}$$

where τ is the tortuosity, D is the molecular diffusion coefficient at temperature 273.15K, and n is a parameter.

3.3 Constitutive equations of the thermal conductivity model

Fourier's law is adopted for the heat conduction flux $\boldsymbol{i}_c$,:

$$\boldsymbol{i}_c = -\lambda_T \nabla T \quad \text{where} \quad \lambda_T = \lambda_{sat}^{S_l} \lambda_{dry}^{(1-S_l)} \tag{20}$$

where λ_T is the soil thermal conductivity, λ_{sat} and λ_{dry} are soil thermal conductivity at the saturated and dry states, respectively.

4 MODEL PARAMETERS, INITIAL AND BOUNDARY CONDITIONS

4.1 Model parameters for the THM analysis

The material used to prepare the soil sample in the experiment is a silty clay, whose the material parameters are collected from reported in the literature experimental data, where parameters for similar soils are given, [4, 1]. Parameters for the coupled thermo-elasto-plastic (TEP) model for typical silty soil are presented in Table 1 and Table 2. The tension stress may induce the tension failure that conducts the FE program to non-converged situation. Therefore the parameters regarding to tensile strength are given higher than the real soil properties. The parameters values are as follows: $\rho = 0.2$ ($^\circ C^{-1}$), $k = 0.01$ (-), $p_{s0} = 0.5$ (MPa).

Table 1: TEP elastic parameters

κ_{io}	κ_{so}	K_{min}	ν	α_{ss}	α_i	α_{sp}	p^{ref}	α_o
(-)	(-)	(MPa)	(-)	(-)	(-)	(-)	(MPa)	$^\circ C^{-1}$
0.01	0.0581	10	0.27	0	-0.01	0.3	0.126	1.0E-05

Table 2: TEP plastic parameters

$\lambda(0)$	r	β	ρ	$\boldsymbol{k}_o$	p^c	M	α	p_0^*	e_0
(-)	(-)	(MPa^{-1})	$^\circ C^{-1}$	(-)	(MPa)	(-)	(-)	(MPa)	(-)
0.115	0.98	0.01	0.2	7.32E-03	0.01	1.12	0.426	0.28	0.88

The basic parameter for temperature evolution and distribution is the thermal conductivity λ, which depends on liquid saturation. Following [14] and [10], the parameters are used as $\lambda_{dry} = 0.7$ and $\lambda_{sat} = 1.3$.

Intrinsic permeability is calculated according to the Kozeny's model based on experimental result from saturated hydraulic conductivity test in THM column at 20°C. Parameters for this model are shown in Table 3.

4.2 Initial and boundary conditions

From the performed in this study experiment it can be seen that cracks occur on the surface of the soil sample. These cracks are radial and circumferential cracks and therefore, in order to assess the expectation of the cracks to appear on the surface of the soil sample during drying, the finite element analysis has to be performed in its 3D formulation. With the 3D model the stress-strain behaviour in condition of tension stress on the surface of the sample can be clearly seen. Because of the existing symmetry in the test sample and for reducing the number of element, thus reducing the cost of the numerical analysis, the geometry of the numerical model was created as one fourth of the whole real soil samples as depicted in Fig. 3. The observation points are selected on the top of the ring (point 2) and on the inside and outside edges of the ring (points 1 and 3). The observation points correspond with the place where cracks occurred in the experiment. The finite element discretization is also illustrated in Fig. 3.

Table 3: Hydraulic parameters

P_0 (MPa)	λ (-)	$\boldsymbol{k}_o$ (m^2)	σ_{T0} (N/m)	ϕ_o (-)	S_{rl} (-)	S_{ls} (-)	D ($m^2 s^{-1} K^{-n} Pa$)	τ (-)	n (-)
0.61	0.446	8.78E-16	0.072	0.481	0.11	1.0	5.6E-7	0.8	2.3

Table 4: Initial condition for THM test

Unit	Porosity (-)	Suction (MPa)	Temperature (°C)	Stress (MPa)
Value	0.48	0.0	20	0.0

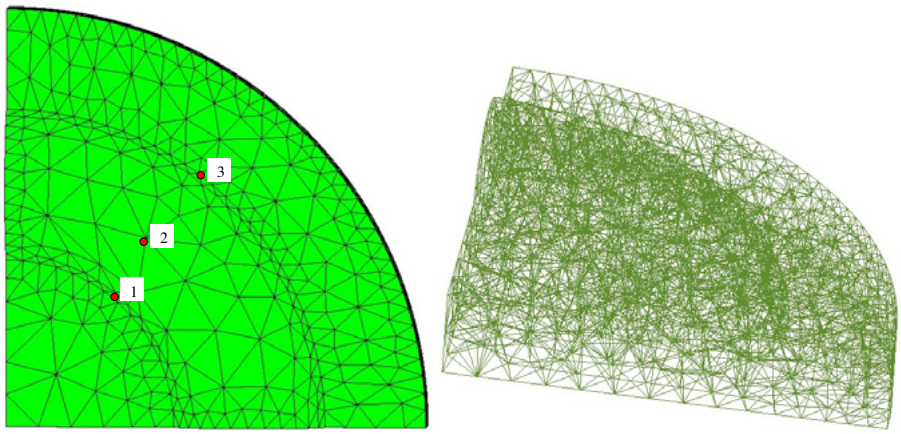

Figure 3: Discretization: (a) View from top. (b) finite element mesh

The simulation is divided into two stages corresponding to the change in the sample environment during the experiment. For the first stage, the applied suction at the upper face is increased gradually from initial 15 MPa to 30 MPa corresponding to 75% ambient room relative humidity. The temperature on the top surface of the sample is kept constant (T=20°C) and equal to the initial temperature of the sample. For the second stage, the applied suction on the upper face is increased gradually from 30 MPa to 45 MPa corresponding to 62% ambient relative humidity after exposing the soil sample to the sun. The temperature on the upper face of the soil sample is increased from 20°C to 37°C in this stage. Fig 4 illustrates the thermal and hydraulic (suction) boundary conditions applied during the simulation. The initial condition is described in Table 4.

The considered time intervals corresponding to the two stages of the experiment are: first stage of 500 hours, corresponding to 20 days keeping the sample in room condition; second stage of 500 hours, corresponding to 20 days keeping the sample outdoor.

5 RESULTS

Figure 5 presents the visualization of degree of saturation after 1000 hours. It is clear that the water saturation on the surface is much smaller than water saturation inside the sample. The difference is even higher at the beginning of the simulation. The reduction of the water saturation by evaporation on the upper surface induces the

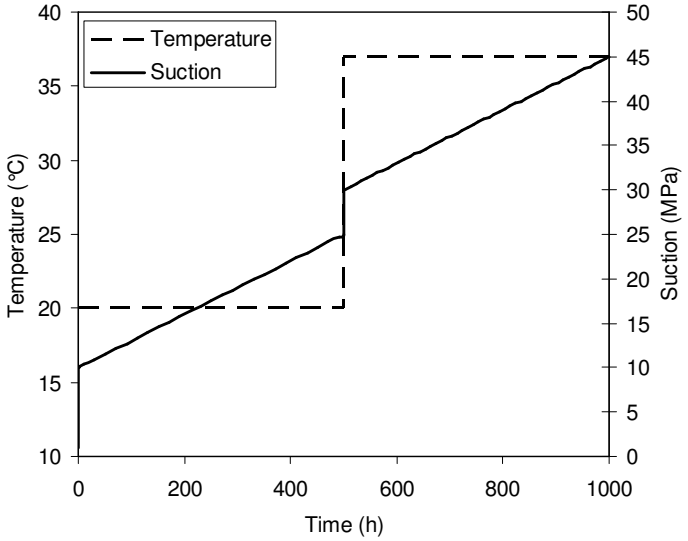

Figure 4: Suction and temperature boundary condition on the upper face of the soil sample

shrinkage phenomenon in this area.

Employing the TEP model, it is possible to simulate the soil shrinkage induced by decreasing suction. The relation between suction and strain is given by equation 5. At the beginning of the simulation, the sample is fully water saturated and no initial mechanical stress is applied. It is coming from the solution that after several days the water saturation at the sample surface is becoming lower than the saturation inside the sample body. Therefore, the shrinkage strain near the sample surface is higher than inside the sample body. This results in a tension stress on the surface of the sample. The obtained tension stress is shown in Fig. 6. It can be seen that the tension stress is more pronounced at the inside and outside edges of the soil ring (track wall). The stress contour analysis reveals that there are lines from the inner edge to the outer edge of the track wall along which the tension stress is higher than at the neighbourhood. This indicates that most probably radial crack will appear along the black lines shown Fig. 6. Thus, the results from the numerical analysis agree with the observation in the experiment.

For analysing the difference between the stress values on the sample surface and the stress inside the sample, we have selected points 1', 2' and 3'. These points are locate at the same place but 2 cm below the respective points 1,2,3. Figure 7a presents the tension stress at the points 1, 2, and 3 with time evolution and corresponding points 1', 2', and 3'. It can be seen that the water saturation decreases rapidly inducing a rapid increase of the surface tension stress. The tension stress at the sample surface later decreases because of the reduction of the difference between the water saturation at the surface and in the sample body, see Fig. 7b. The same process is repeated in the very beginning of the second stage, when the applied suction and temperature increase to 45 MPa and 37°C,

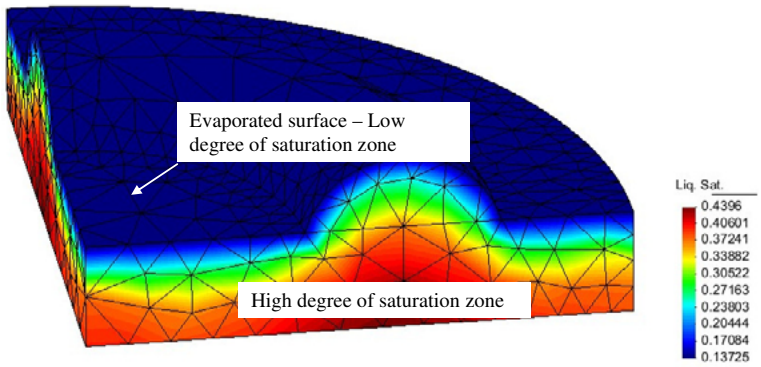

Figure 5: Distribution of the degree of saturation after 1000 hours.

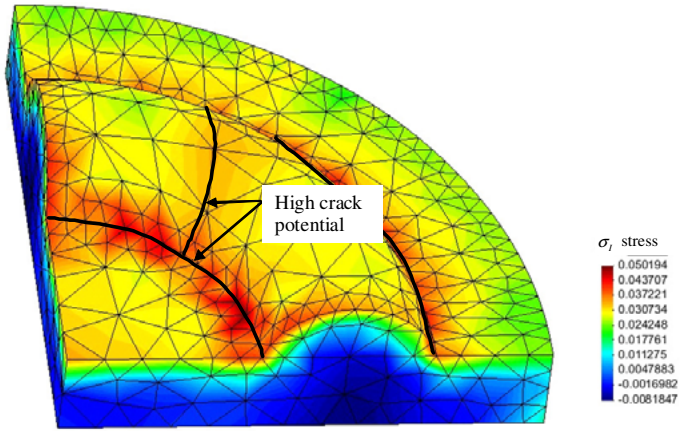

Figure 6: Distribution of the maximum principal stress (MPa) after 1000 hours.

respectively. The net tensile mean stress increases for a short time at the beginning of the second stage, then slowly decreases.

Figure 7b presents the evolution of the water saturation during the test at point 2 and point 2', and at point 2" located at depth of 7 cm below the point 2. The degree of saturation on the surface (point 2) decreases rapidly to 0.2, whereas at the points 2' and 2" in the body of the soil sample the degree of saturation decreases slowly. In point 2 at the beginning of the stage 2 there is a small decrease of water saturation, but the change of the water saturation in points 2' and 2" is undistinguished. The variation of the degree of saturation suggests an increase of the tension stress on the surface of the sample. The degree of saturation of the three observation points is expected to be the same at infinite time.

6 CONCLUSIONS

An experimental setup and numerical simulation using coupled THM analysis are presented and discussed. The experiment and the numerical modelling of the experimental

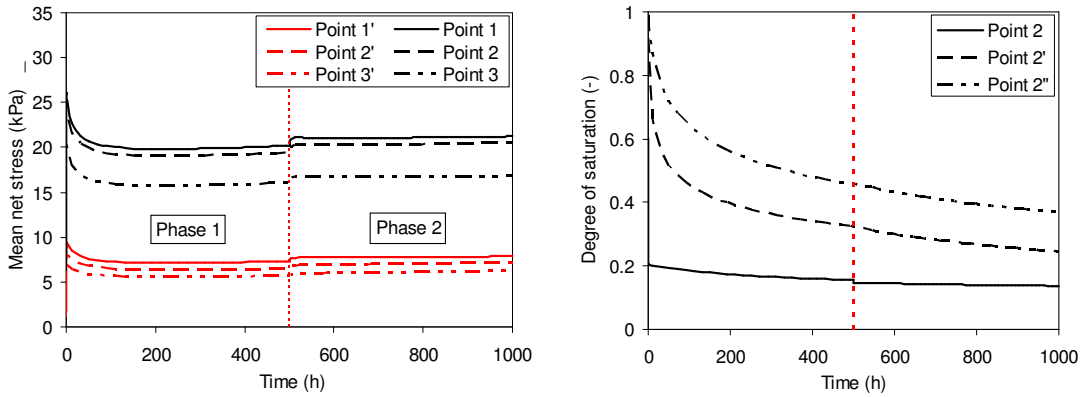

(a) (b)

Figure 7: (a) Mean net stress in points 1,2,3 and 1', 2', and 3'. (b) Evolution of the degree of saturation with time.

setup are done in order to analyse the initiation of cracks on the surface of dinosaur's footprints. The stress analysis shows that the potential for crack appearance exists on inside and outside edges of the soil ring (track wall), and along the radial direction of the ring. The results show an agreement between observed cracks and simulated tensile stress concentrators. It can be concluded that the high tensile stress on the footprint's surface that appears due to soil shrinkage phenomenon is most probably the reason for the appearance of cracks in radial and circumferential directions.

References

[1] E.E. Alonso, A. Gens, and A. Josa. A constitutive model for partially saturated soils. *Géotechnique*, 40(3):405–430, 1990.

[2] Z.T. Bieniawski. Mechanism of brittle fracture of rock: Part I: theory of the fracture process. *International Journal of Rock Mechanics and Mining Sciences & Geomechanics*, 4(4):395 – 406, 1967.

[3] DIT-UPC. *CODE_BRIGHT user's guide*. Universitat Politècnica de Catalunya, Barcelona, Spain, 2009.

[4] F. Geiser. *Comportement mécanique dún limon non saturé - Étude expérimentale et modélisation constitutive*. PhD thesis, PhD Thesis. Lausanne, EPFL, 1999.

[5] A. Gens. Constitutive laws. In A. Gens, P. Jouanna, and B. Schrefler, editors, *Modern issues in non-saturated soils*. Springer-Verlag, 1995.

[6] L. N. Germanovich, R. L. Salganik, A. V. Dyskin, and K. K. Lee. Mechanisms of

brittle fracture of rock with pre-existing cracks in compression. *Pure and Applied Geophysics*, 143(1–3):117–149, 1994.

[7] Ole Graversen, Jesper Milàn, and David B. Loope. Dinosaur tectonics: A structural analysis of theropod undertracks with a reconstruction of theropod walking dynamics. *The Journal of Geology*, 115:641–654, 2007.

[8] Simon J. Jackson, Martin A. Whyte, and Mike Romano. Laboratory-controlled simulations of dinosaur footprints in sand: a key to understanding vertebrate track formation and preservation. *PALAIOS*, 24:222–238, 2009.

[9] J. Milàn and R.G. Bromley. True tracks, undertracks and eroded tracks, experimental work with tetrapod tracks in laboratory and field. *Palaeogeography, Palaeoclimatology, Palaeoecology*, 231:253–264, 2006.

[10] L. Nguyen-Tuan, M. Datcheva, and T. Schanz. Numerical simulation and back analysis of coupled thermo-hydro-mechanical behavior of sand-bentonite mixture. In K. Guerlebeck and C. Koenke, editors, *18th Int. Con. on the Application of Computer Sci. and Math. in Architecture and Civil Eng.*, page paper 184, Weimar, Germany, 2009. ISSN: 1611 - 4086.

[11] S. Olivella, J. Carrera, A. Gens, and E. E. Alonso. Porosity variations in saline media caused by temperature gradients coupled to multiphase flow and dissolution/precipitation. *Transport in Porous Media*, 25(1):1–25, October, 1996 1996.

[12] S. Olivella, J. Carrera, A. Gens, and E.E. Alonso. Non-isothermal multiphase flow of brine and gas through saline media. *Transport in porous media*, 15:271 – 293, 1994.

[13] S. P. Olivella. *Nonisothermal multiphase flow of brine and gas through saline media*. PhD thesis, Universitat Politècnica de Catalunya, 1995.

[14] M. Sánchez, A. Gens, and S. Olivella. Thermo-hydro-mechanical modelling of low permeability media using a double-porosity formulation. *Mecanica Computacional*, XXIII(7):733 – 754, 2004.

[15] M. Th. van Genuchten. A closed-form equation for predicting the hydraulic conductivity of unsaturated soils. *Soil Sci. Soc. Am. J.*, 44:892–898, 1980.